ASSESSMENT OF THE ATMOSPHERIC CHANNEL FOR SHORT (Ka-BAND and OPTICAL) WAVELENGTHS

Sabino Piazzolla
Jet Propulsion Laboratory
California Institute of Technology
Pasadena, CA 91109
sabino.piazzolla@jpl.nasa.gov

Abstract— **Atmospheric turbulence under clear sky conditions is an impairment of the atmospheric channel that greatly affects propagation of optical signal in the troposphere. The turbulence manifests itself in a number of forms within the optical domain, from the twinkling of a star in a clear night, to resolution degradation in a large aperture telescope. Therefore, a body of analytical, numerical, and experimental tools has been developed in optics to study, simulate, and control effects of atmospheric turbulence on an optical signal. Incidentally, there has been an increasing demand for high data rate returns from NASA missions which has led to envision utilizing a carrier signal in the Ka-Band range. The impact of atmospheric turbulence effects must be evaluated and considered for this frequency domain. The purpose of this work is to show that when the turbulence strength from the optical case to the Ka-Band case is properly scaled, one can apply the same mathematical/simulation developed for optical to predict turbulence effects within the Ka-Band domain. As a demonstration of this principle, we present how the scintillations of a Ka-Band downlink return of a deep space signal was successfully reproduced through wave-optics simulation.**

.

1. INTRODUCTION

NASA is facing new challenges as it enters a new paradigm in its architecture, mainly driven by the demand of higher data return rates. At the same time, several key parameters of NASA's antenna network are also evolving, *e.g.*, data volume will increase at least 10 to 100 times if not higher and the number of missions per year may experience a four-fold increase. The desire for higher data rates has already encouraged rapid development of the Ka-band systems and services for deep and near space applications. Such a migration to higher frequencies, however, comes in contrast to the fact that the RF link is much more susceptible on the status of the atmospheric channel. For instance, atmospheric absorption may increase at such frequencies and cloud coverage can be not only a source of additional link loss but even link blockage. Moreover, clear air turbulence effects can be more evident at Ka-Band frequencies with a number of additional losses related to signal fading caused by scintillations and fluctuations in the angle of arrivals. However, all these (high frequency related) atmospheric impairments have long been studied in the optical domain where the dynamics of atmospheric channel effects are even more dramatic. For instance to avoid link blockage due to cloud coverage, single site and spatial diversity statistics have been extensively examined [1]. It is, however, in the field of clear sky turbulence studies that Ka-Band techniques can adopt a lot from optics. The need to reduce these detrimental limitations, especially for large aperture optical telescope observations, has led to numerous developments in the study, simulation and correction of turbulence effects in optics. The aim of this paper is to demonstrate how the wealth of turbulence studies in the optical regime can be easily adapted to suit Ka-Band. As a demonstration, it will be shown how wave-optics simulation can be used to study signal scintillation in Ka-Band downlink signal returns form a deep/near space probe. The organization of this work is the following. In Sect. 2 a basic introduction to clear air turbulence will be provided including the description of the main parameters necessary to understand the problem. In Sect. 3 wave-optics simulation technique will be described along with a number of simulation results. Summary and conclusion will be presented in Sec. 4.

2. CLEAR AIR TURBULENCE: COMPARISON BETWEEN KA-BAND AND OPTICAL WAVELENGTHS

A. Description of clear air turbulence.

When a high frequency EM wave (such as a Ka-Band or Optical) propagates through the atmosphere, it is greatly affected by spatial variations of the atmospheric refractive index. These variations are related with the fluid type motion of the air; when atmospheric flow exceeds a certain critical level, its nature changes from laminar to a chaotic one where the energy is transferred from vortices of relatively large to small scales until it is dissipated as heat. This chaotic regime is defined as clear air turbulence and it is best described with a statistical approach. As an example, for a homogeneous and isotropic atmosphere, the variation of the refractive index ($n(\boldsymbol{r})$) can be properly represented by the refractive index structure constant C_n^2, which is related to the refractive

index structure function $D_n(\boldsymbol{r})$, as

$$D_n(r) = D_n(r_1 - r_2) = <[n(r_1) - n(r_2)]^2 >= C_n^2 r^{2/3}, \text{ (Eq. 1)}$$

where r_1 and r_2 indicate the observation points, the term <( )> stands for the averaging operator, while C_n^2 is dimensionally described by [m$^{-2/3}$].

Air turbulence can affect the propagation of a beam in a number of fashions, as illustrated by Fig. 1. First, because a propagating beam experiences a spatially varying refractive index, the wavefront can be distorted and corrupted, with resulting spatial randomness in its phase. Next, due to refractive index irregularities, the wave intensity can be locally focused and defocused at the aperture such that

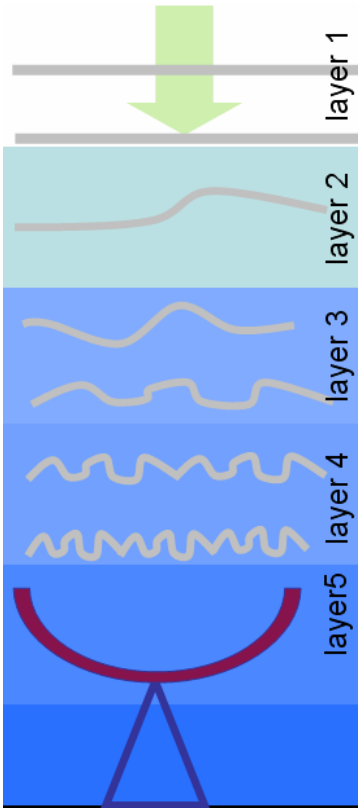

Fig. 1. Conceptualization of a plane wave propagating through the atmosphere. As the beam propagates, its wavefront gets more corrupted due to atmospheric turbulence. For simulation purposes, one can divide the atmosphere in a number of layers of constant (within the same layer) turbulence strengths.

the fluctuations, or scintillations, of the average signal are shown. Finally, other evident effects of the atmospheric turbulence are random variations in the angle of arrival and (especially for an optical beam) broadening of the point spread function of the receiving telescope.

B. Figue of Merits.

Providing a functional description of the turbulence effects on the propagating beam is not a simple problem. Complexity in the analysis of clear air turbulence arises from the fact that solutions of Maxwell's equations are also statistical in nature when given a statistical medium. Using the Rytov method [2], one can find the solutions of Maxwell's equation by expressing the electric field, E, in scalar representation as

$$E = \exp(\chi + jS) \text{ (Eq. 2)},$$

where χ is defined as the random log-amplitude of the wave, and S describes the phase of the electric field.

Solutions from the Rytov method are particularly helpful in expressing the important figures of merit of a wave propagating, such as the scintillation index and the atmospheric coherence length (defined later).

The scintillation index σ_I^2, is the variance of the normalized intensity I of the wave and it is defined as

$$\sigma_I^2 = <[I - < I >]^2 > / < I >^2 \qquad \text{(Eq. 3)},$$

within the weak fluctuation regime, which occurs when $\sigma_I^2 <$ 1, one can write

$$\sigma_I^2 = \exp(4\sigma_\chi^2) - 1 \approx 4\sigma_\chi^2 \qquad \text{(Eq. 4)},$$

The term $\sigma_{x,}^2$ named as Rytov variance, represents the variance of the log-amplitude of the wave. For a downlink return signal where the electromagnetic wave is represented by a plane wave, one can express the Rytov variance as

$$\sigma_\chi^2 = 0.56k^{7/6} \sec^{11/6}(\theta) \int C_n^2(z) z^{5/6} dz \qquad \text{(Eq. 5)},$$

where k is the wavenumber, θ is observer the zenith angle , z is the elevation above sea level (m), and the integral is performed from the receiver altitude to the upper altitude limit of the troposphere (~30 km).

Concerning the phase distortion of a downlink plane wave, the term r_o, instead, indicates the aperture (over the wavefront) where phase aberration is 1 rad in rms:

$$r_o = [0.423k^2 \sec(\theta) \int C_n^2(z) dz]^{-3/5} \text{ (Eq. 6)}.$$

In the Literature, r_o is referred to as the atmospheric coherence length or Fried parameter [3].

The scintillation index expressed in Eq. 5 refers to the case of a point receiver where the diameter D of the receiver aperture is much smaller than r_o. For a large collection aperture, the signal scintillation index is reduced due to an averaging effect of the receiver area that integrates the overall signal irradiance. The aperture averaging factor, where $A_v < 1$, is described in a simple analytical form in Ref. [4] as

$$A_v = \frac{1}{1 + 1.1(D^2 \cos(\theta) k / 2\pi h_o)^{7/6}} \text{ (Eq. 7)},$$

in which the term h_o is

$$h_o = [\frac{\int C_n^2(z) z^2 dz}{\int C_n^2(z) z^{5/6} dz}]^{6/7} \text{ (Eq. 8).}$$

C. Wavelength Scaling.

As described so far, one can notice that the analytical treatment of clear turbulence effects is independent of the wavelength of the wave propagating through the atmosphere. Thus one may apply the same treatment for both optical and Ka-band signals. On the contrary, the magnitude of the effects (e.g. scintillation, atmospheric coherence length, etc) is dependent on the wavelength and the refractive index structure parameter. From an analysis of Eq.'s 5 and 6, one can visualize that a beam at shorter wavelengths, as those in the optical domain, will experience greater interaction with the turbulent medium with resulting larger scintillation index and shorter atmospheric coherence length. At the same time, the magnitude of the refractive index structure constant plays a relevant role in the amplification of the atmospheric turbulence effect; a larger C_n^2 leads to larger scintillation index and a smaller atmospheric coherence length. Theoretical and experimental data, such as those in Ref [5], indicate that the refractive index structure constant in the optical domain mainly depends on temperature and atmospheric pressure. In the millimetric wave domain, C_n^2 greatly depends on other factors such as air humidity. Experimental measurements also indicate [5] that at low elevation, C_n^2 for Ka-Band can be, *ceteris paribus*, up to three orders of magnitude larger than that for the visible domain. If we examine the vertical profile of C_n^2, it is evident that it is larger for the boundary layer at low altitude and rapidly decreases with higher elevation where the air density is reduced.

While greatly dependent on the geographic location, time of day, and day of the year, models describing the vertical profile in optical domains have been extensively reported [6]. Among them, one of the most used is the so called Hufnagel-Valley [6]:

$$C_n^2(z) = 1.7x10^{-14}\exp(-z/100) + 2.7x10^{-16}\exp(-z/1500) + 5.94x10^{-3}(v/27)^2(10^{-5}z)^{10}\exp(-z/1000) \quad (Eq.10),$$

where v is rms wind speed (m/s) at higher altitudes.

In the case of Ka-Band, there is a lack of data concerning the modeling of the C_n^2 profile, although one would expect that C_n^2 should assume values larger than that for optical wavelengths. Therefore, we have assumed that the C_n^2 profile for the Ka-Band is a multiple of the Hufnagel-Valley of Eq. 10 in our simulations.

3. WAVE-OPTICS SIMULATION OF A KA-BAND RETURN SIGNAL

A. Wave-optics Simulation of Ka-Band Downlink Description.

As described in Sect. 2, there are no conceptual differences between turbulence effects in the optical domain and Ka-Band, beside the fact that a propagating wave has different wavelength and the refractive index structure constant may have different values. This suggests that one can largely apply, for the Ka-Band, all the theories and simulation techniques extensively used in optics to study/characterize the effects of turbulence. Among these techniques, wave-optics simulation has largely been used with success to simulate and study the effects of clear air turbulence for a propagating optical beam in fields such as adaptive optics, optical tracking, and laser comm [7]. Compared to analytical methods, wave-optics numerically simulates the propagation of a two dimensional wavefront of an electric field sampled in a spatial grid described by an array of **NxN** elements over an area of interest [8]. In a wave-optics simulation, the atmosphere along the direction of propagation is divided into a number of **M** layers, Fig. 1. The propagation of the two dimensional wavefront from the beginning of one layer to the beginning of the next takes place in two steps: first the phase of the spatially sampled electric field is modulated by a phase screen whose strength is determined by the average C_n^2 in the layer. This phase screen describes the phase aberrations experienced by the propagating wave that are induced by the atmospheric turbulence within the layer. Next the electrical field is propagated to the beginning of the next layer using fast-Fourier-transform techniques [8]. The propagation process is repeated through the layers until the wave reaches the antenna aperture where the wave intensity is integrated over the antenna surface, Fig. 1. This procedure describes only the propagation of the wave in one single realization at the initial time t_1. To simulate the propagation over the next time interval, the process is updated to the next time step $t_1 + \Delta t$, in which the phase screen of each layer experiences a spatial shift as $v_T \Delta t$, where v_T is the transversal component of the wind speed. Once the phase screens are updated, the propagation through the **M** layers is repeated and the wave intensity is again collected by the antenna aperture and the power at the time $t_1 + \Delta t$ is calculated. The algorithm (phase screen update and propagation) is repeated n-times until the simulation reaches the final simulation time $t_f = t_1 + n\Delta t$.

To validate the application of the wave-optics method for Ka-Band propagation, it was attempted to replicate the atmospheric turbulence induced effects over a Ka-Band signal carrier from a deep space mission. In particular, a 32 GHz return signal from the Cassini spacecraft measured with a 34m Beam-Waveguide antenna at the JPL/NASA Deep Space Network center Goldstone, CA [9]. To study and replicate measurable signal scintillations of meaningful size, a pass at relatively low elevation angle was considered. A pass at elevation angle of 14° degree was chosen, and incidentally, the measured transversal wind speed at the ground was 0.39 m/s. The normalized intensity of the return signal is illustrated by the solid line in Fig. 2 where the evolution of 10 minutes of signal is reported. From Fig. 2, one can clearly notice that the return signal is characterized by sub-hertz components, attributed to the scintillation of the signal, while higher frequency components are attributed to different causes (e.g. thermal noise, mechanical related noise

etc.). To replicate the return signal using a wave-optics simulation, the troposphere was divided into 8 layers of different strengths (to be specified later) and a spatial grid of 1024x1024 elements was used to represent the electric field of the downlink plane wave. A key element of the simulation was the determination of the C_n^2 profile, where following rationale was used. First, the signal scintillation index measured (and averaged) by the 34m antenna was calculated based on the measured return signal. Next, using Eq. 7, the aperture averaging of the antenna was computed. The resulting scintillation index and aperture averaging factor were then combined to derive the Rytov variance. Finally, a multiplier of the Hufnagel-Valley profile of Eq. 10 was determined by equating the derived Rytov variance to that from the measured/derived in the signal return using Eq. 5 and the so derived C_n^2 profile. The multiplier for this particular simulation was found to be 1800. Having defined the C_n^2 profile, the wave-optics simulation was performed with a time step of Δt=0.25 s.

B. Simulation Results

Figure 2 clearly compares results of the simulation (dashed line) with the measured signal (both received powers represented are normalized by their respective average value). While the wave-optics simulation did not present effects of higher frequency disturbances as seen in the original return signal, it effectively replicated the signal variation due to clear air scintillation as also confirmed by the scintillation index that was 0.0091 for the simulation and 0.0097 for the measured signal.

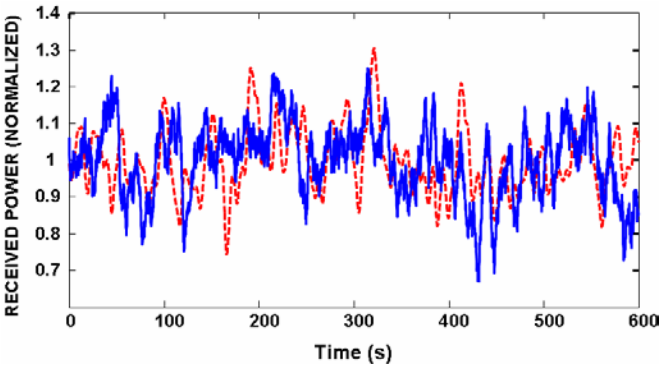

Fig. 2 Ka-Band (32 GHz) signal return from deep space probe. The receiver power is normalized by the average value. Elevation angle is 14° and antenna aperture 34m. The measured return signal (solid line) is compared with the simulated one (dashed line). The C_n^2 profile used in the simulation is 1800 times the Hufnagel-Valley model and the transversal wind speed is 0.39 m/s.

An even better validation of the wave-optics simulation comes from the comparison of the power spectral density between the two signals (measured and simulated) as shown in Fig. 3. In this case, there is a great agreement in the power contributions in the sub-hertz range up to 0.5 Hz, with some difference around 1 Hz of little contribution in power.

Wave-optics simulation of the Ka-Band signal can be also extremely useful also in determining the effects of clear air turbulence for receiver antennas of different apertures. As demonstration of this concept Fig. 4 illustrates 10 minutes of the dynamics of the (normalized) power received by 6, 18, and 34 meter aperture antennas. This example also used the same carrier signal frequency, elevation angle and turbulence strength as the data in Fig.2.

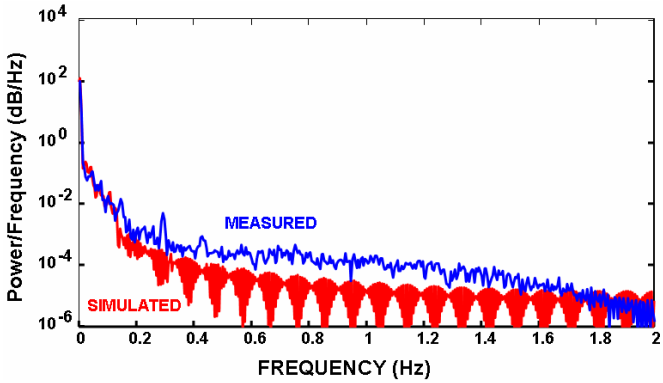

Fig. 3 Comparison between the power spectral density of the measured signal and the simulated one represented in the time domain in Fig. 2. There is an excellent agreement in the low frequency range pertinent to effects of scintillation at the receiver.

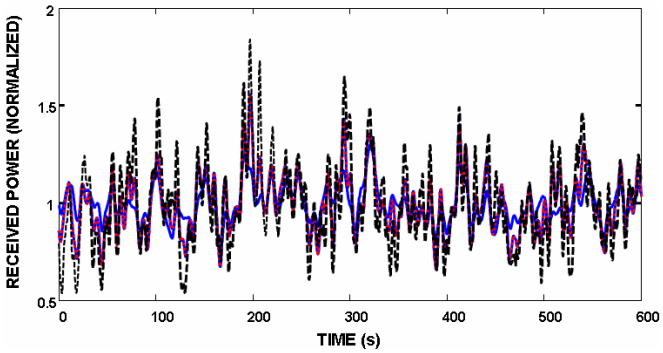

Fig. 4 Simulation of the Ka-Band (32 GHz) signal return from deep space probe. Turbulence conditions are as those in Fig. 2. Elevation angle is 14o and antenna apertures are 34m (solid line), 18m (dashed line) and 6 m (dotted line). Signal power of each realization is normalized by its average values.

Due to the smaller aperture averaging effects of smaller antennas (less than 34m), the scintillation indices were 0.043 for the 6 m antenna, 0.023 for the 18 m, and (again) 0.0091 for the 34 m antenna. Such a difference in the scintillation indices of the three antennas is also reflected in the signal statistics for the three antennas themselves. Figure 5 represents the cumulative distribution function (CDF) for the three different aperture sizes which presents interesting performances for the antennas and the fade statistics. For instance, if one hypothetically considered a system driven limit of 1 dB or less of fade due to signal scintillation, according to the data in Fig. 5 one can deduce that this limit is met 99% of the time for the 34 m antenna, 91% of the time for the 18 m antenna and only 82% of the time for the 6 m antenna. In Fig. 5 the cumulative distribution function of the measured return signal for the 34m antenna is plotted; the shape is extremely close in form to the one obtained from the wave optics simulation of the same antenna size.

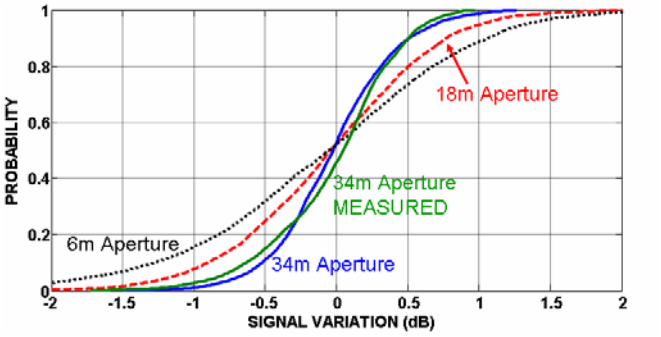

Fig. 5 Cumulative distribution function for antennas of 34, 18, 6 meter apertures for the 32 GHz signal return. The elevation is 14°, the turbulence conditions are as those in Fig. 2. Simulation results from the wave-optics run are indicated with those of the actual measured signal.

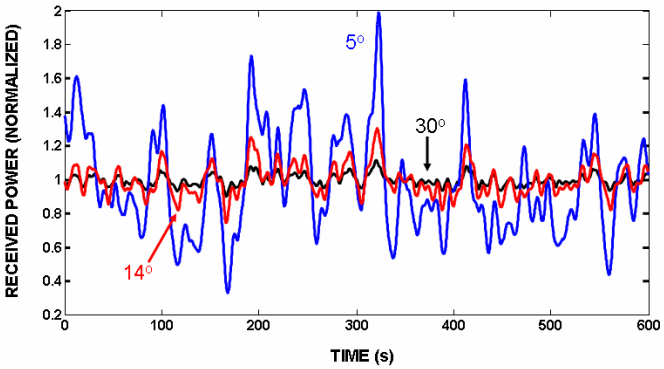

Fig. 6 Simulation of the Ka-Band (32 GHz) signal return from deep space probe. Turbulence conditions are as those in Fig. 2. Elevation angles are 5°, 14° and 30°. The antenna diameter is and 34m for all three realizations. Signal power of each realization is normalized by its average values.

As indicated in Eq. 5, scintillations of the signal are greatly dependent on the elevation angle since different elevation angles correspond to different path lengths a downlink signal must traverse through the atmosphere. Therefore to describe the signal dynamics at different elevation angles, a number of wave-optics simulations were executed for a 32 GHz return downlink signal collected by a 34 m antenna at elevation angles 5, 14, and 30 degrees. The C_n^2 profile used in these simulations was the same as the previous one (Hufnagel-Valley x 1800). Time dependent realizations of the signal are represented in Fig. 6, that indicate how scintillation effects are more pronounced (scintillation index of 0.12) reaching fade levels of multiple dB's at lower elevation angles, 5°. However, for the same turbulence strengths but at an elevation angle of 30°, most of the signal fadings and power surges are reduced (scintillation index of 0.0012). Figure 7 displays the results of the different elevation angle simulations in CDF format. One can observe that a system limit of 1 dB fade in the received signal is met almost 100% of the time at 30° elevation, 99% of the time at 14°, and only 70% of the total time at an antenna elevation of 5°.

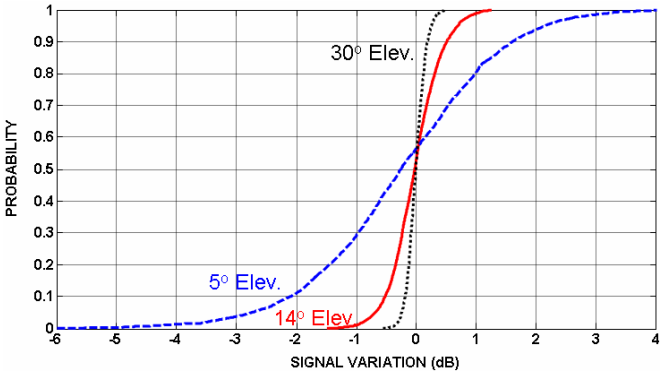

Fig. 7 Cumulative distribution function of the signal return for 34m antenna Signal frequency is 32 GHz signal while turbulence conditions are as those in Fig. 2. The elevation angles are 5°(dashed line), 14° (solid line) and 30°(dotted line). These CDF's are obtained from the time wave-optics realization depicted in Fig. 6.

4. SUMMARY AND CONCLUSION

This work has illustrated how wave-optics simulation can be successfully used to simulate the effects of clear sky turbulence on a Ka-Band return signal. Given a proper profile of the turbulence, wave-optics simulation was shown to effectively replicate a measured signal return from deep space in term of signal dynamics, power spectral density, scintillation index, and CDF. Extension of this method can also be utilized to understand other clear turbulence effects relating to return link like variations of angle of arrival and antenna aperture scaling. Moreover, one may suggest extending the use of wave-optics simulations for other Ka-Band applications such as uplink/downlink array where the turbulence induced phase variation of wave at each terminal of the array can be cause performance degradation of array system itself.

ACKNOWLEDGMENT

The Author would like to thank Dr. Kar-Ming Cheung, Dr. David Morabito and Janet P. Wu for the support and technical discussions provided during the preparation of this work.

The research described in this paper was carried out at the Jet Propulsion Laboratory, California Institute of Technology, under a contract with the National Aeronautics and Space Administration.

REFERENCES

[1] S. Piazzolla, S. Slobin," Statistics of link blockage due to cloud cover for free-space optical communications using NCDC surface weather observation data," in Proc. SPIE Vol. 4635, 2002.

[2] V.I. Tatarskii, *Wave Propagation in a Turbulent Medium*, (Mc.Graw-Hill, New York, 1960).

[3] D. L. Fried, "Optical Resolution through a Randomly Inhomogeneous Medium," *J. Optic. Soc. Am.*, 56, 1372-1379 (1966)

[4] H. T. Yura and W. G. McKinley, "Aperture averaging of scintillation for space-to-ground optical communication applications," *Appl. Opt.* **22**, 1608-(1983)

[5] Arnold Tunick and Henry Rachele," Estimating effects of temperature and moisture on C_n^2 in the damp unstable boundary layer for visible,

infrared, radio, and millimeter wavelengths," in Proc. SPIE Vol. 1688 Atmospheric Propagation and Remote Sensing (1992)
[6] F. G. Smith, The Infrared and Electro-Optical System Handbook, Vol. 2, (SPIE Optical Engineering Press, 1993).
[7] D. M. Strong, E. P. Magee, and G. B. Lamont, "Implementation and test of wave optics code using parallel FFT algorithms, Proc. SPIE 4167, 34 (2001).
[8[S. Coy, "Choosing mesh spacings and mesh dimensions for wave optics simulation," Proc. SPIE 5894, 589405 (2005).
[9] D. D. Morabito, "Detection of Tropospheric Propagation Effects from Deep Space Links of the Cassini Spacecraft," accepted for publication in *Radio Science*